Tensile behaviour of magnesia carbon refractories

N. Schmitt [a],*, Y. Berthaud [a], J. Poirier [b]

[a]*LMT-Cachan, ENS de Cachan (CNRS) Université Paris 6, 61, Ave. du Président Wilson, F94235 Cachan Cedex, France*
[b]*CRDM/SOLLAC, Grande Synthe, F-59 381 Dunkerque Cedex, France*

Abstract

The determination of the Young's modulus and the tensile strength of heterogeneous refractories are the subjects of this paper. Great differences have been observed for a similar material according to both the usual tests performed and the interpretation proposed to define these properties. The causes of the discrepancies of the Young's modulus under compression and tensile loading are examined in detail. Then, it is shown that (i) the accuracy measurement of the deflexion in the bend test with a particular device and (ii) the integration of the shearing distorsion in the calculation of the deflexion by the classical beam theory, allow for finding the appropriate value of the Young's modulus. The classical definition of the modulus of rupture (*M.O.R.*) is also examined. Considering a nonlinear behaviour of the refractory, it is shown by finite element analysis of the beam, that the *M.O.R.* overestimates the tensile strength. © 2000 Elsevier Science Ltd. All rights reserved.

Keywords: Elastic modulus; Mechanical properties; MgO-C; Refractories; Strength

1. Introduction

Magnesia-carbon refractories used in steel converter L.D. linings undergo high temperature during the steel-making process. Thermal shock occurring during the first heating, and the cyclic changes of the temperature due to steel manufacturing induce thermal stresses that can lead to flake failures reducing the lining time-life.[1] Hasselman's classical criteria[2] and Finite Element Analysis[1] are generally used to predict their structural integrity. In these analyses, Young's modulus and the tensile strength are most important mechanical parameters to choose the optimal composition of refractories.

In this paper, it is shown that the interpretation of the measures obtained by the classical experimental tests leads to different values of Young's modulus and of the compression and tensile strengths. The difficulty is increased because these refractories present great contrasts of mechanical behaviour and properties. Some answers are proposed to find the true properties to introduce in such analysis.

At first, a short presentation of refractories is given. Two types of material are examined, one bound with resin, the other one with pitch. Then, the uniaxial behaviour of such materials is shown. It reveals the existence of a non-symmetrical compression-tensile behaviour and the presence of a non linear domain even for extremely low strains. The differences of behaviour of the two types of materials are shown. The principal parameters of these refractories are determined. In particular, the meaning of Young's modulus is discussed and complementary analysis are made to understand the discrepancies observed.

In the next part, the tensile properties of the materials are derived by a three-point bend test especially designed and are compared with that of previous tests. The limitations of the classical formulae used to obtain Young's modulus and the tensile strength are remembered. Finally, the effect of the nonlinear behaviour of material, which partially explains the differences between the tensile properties obtained from tensile and three-point bend tests, is analysed with a Finite Element Method (FEM).

2. Presentation of the refractory materials

The industrial refractories tested in this study were composed of magnesia aggregates and a binder (phenolic resin or pitch) containing in some cases graphite and/or additional metallic elements (aluminium, silicon). Fig. 1

---

* Corresponding author.

shows an example of such microstructure. The magnesia aggregates were formed by sintering of crystallites with weak interfaces. The magnesia grain size varied from less than one half millimeter up to five millimeters. The other compound (SiO_2, AlO_3) impurities were very thin and scattered in the carbon binder.

The manufacturing process of bricks depended on the nature of the binder. For resin binder refractories, the components were mixed and shaped into bricks at low temperature (20–50°C) and under high pressure (nearly 100–1000 MPa). Then the bricks underwent heat treatment (100–200°C) to start the polymerisation of resin[3] and to eliminate residual water and phenols. For pitch binder refractory, the elements were mixed at temperatures between 120–150°C and shaped into bricks under high pressure (100–1000 MPa).

More often than not a heat treatment at higher temperature is carried out (300–500°C) to start the pyrolysis. Lubala et al.[4] have shown that physico-chemical transformations appear during the heating of the bricks at high temperature (up to 1000°C) leading to an elimination of volatiles and the creation of a rigid carbon skeleton. Such transformations affect the mechanical behaviour as shown by Fitchett et al.[5] The materials tested were heated at 500°C for 10 h to eliminate most of the volatiles. Table 1 gives the composition of the materials after the heat treatment.

3. Uniaxial compression–tensile behaviour

3.1. Experimental results by compression tests

The tensile and compression mechanical data of refractories are mainly obtained by three-point bend tests and compression uniaxial crushing tests.[6] At first,
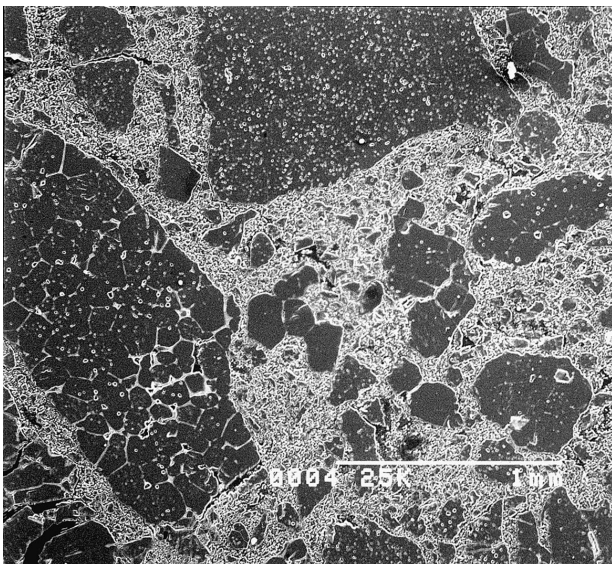
in order to understand the behaviour of these materials compression tests were carried out.

Large specimens (100 × 100 × 250 mm) were tested on a 250 kN servo hydraulic testing machine. The faces of the specimen were machined to impose a high parallelism. The loading had been imposed through machined platens, one of which had a free rotation joint to minimise the effect of bending. Four gauges were glued on the four faces of the specimen to measure an average longitudinal strain and two other gauges were glued perpendicularly to measure Poisson's ratio. The strain rate applied during the loading was equal to -1.5 10^{-5} s^{-1}.

Fig. 2 shows the differences of behaviour for two types of refractory submitted to the same monotonic loading :

- material A with a resin binder exhibited a nonlinear ductile type behaviour, similar to classical concrete behaviour,[7]
- material B with a pitch binder had a significantly more brittle behaviour. Both the stiffness and the ultimate strength were four times higher than those of material A.

Table 1
Composition of magnesia-carbon refractories

Materials	MgO-C resin binder (A)	MgO-C pitch binder (B)
Composition	% weight	% weight
MgO	82.9	91.4
CaO	1.3	1.1
SiO	0.7	∼0
Al_2O_3	0.6	∼0
C	13.1	5.6
Density	2.83	3.07

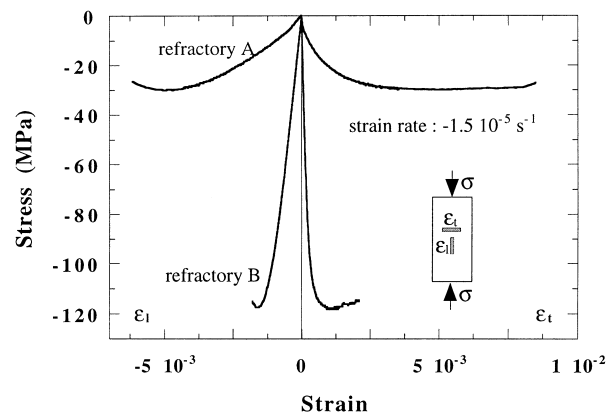Fig. 1. Micrograph of a magnesia carbon refractory.

Fig. 2. Compression behaviour for materials A and B under monotonic loading.

The load–unload cycles shown in Fig. 3 revealed the existence of residual strain, hysteresis and reduction of stiffness due to degradation occuring in material B. These phenomena were due to microcracks initially present in the binder or created during the loading which propagated inside the binder and around the grains. Also debounding of the aggregate-binder interface and weak crystallites interphases in the magnesia grains were observed by observations under scanning electron microscope. Other causes can probably be involved like microplasticity in the binder or release of the residual stresses introduced during the manufacturing as mentioned by Evans.[8]

The same kind of behaviour was observed for material A, but these phenomena were clearly more marked. Indeed, the binder was softer and the microplasticity was more important than in the pitch binder. Moreover, material A contained graphite flakes in which two sets of microcracks parallel and perpendicular to the layers were observed. As suggested previously by Cooper et al.[9] sliding and crumpling of these flakes would also contribute to the higher nonlinearities observed.

The main data are reported in Table 2. Taking a closer look, it appeared that the initial linear domain generally used to determine the value of Young's modulus E_c was not well defined even for low strains especially for material A. The values of Young's modulus reported in

Table 2 corresponded to a secant modulus measured for axial strain of $-5\ 10^{-4}$.

3.2. Experimental results by tensile tests

The tensile behaviour is more difficult to handle because of the strain localisation that occurs early during the tensile load and induces the propagation of a single crack through the specimen. A special setting-up to delay the inception of microcracking, developed in the past by several authors[10,11] was used in this study.

Aluminium bars were stuck on the lateral faces of the specimen (Fig. 4). The load was imposed on the refractory through elastic bars which were fixed on the grips of the test machine. The central zone of the specimen was mainly under an uniaxial tensile stress which is deduced from the equilibrium of the specimen. Strain gauges were stuck both on the bars and the refractory to check the homogeneity of the strain. The same strain rate as in compression tests was applied during loading.

Fig. 5 shows the deduced stress–strain curves for refractories A and B under the assumption that the specimen is a parallel system of refractory and alumina bars with perfect interface between them. A linear behaviour was observed at the beginning of the load. It was followed by hardening-softening regimes which arose from the initiation of microcracks around the aggregates all over the specimen, their propagation into the binder and then their coalescence to two or three macrocracks. Boudon-Cussac et al.[12] have shown that for this test, there exist a debounded zone of the interface near the cracks. In fact, the softening include non-linearities due to both refractory and weak interface.
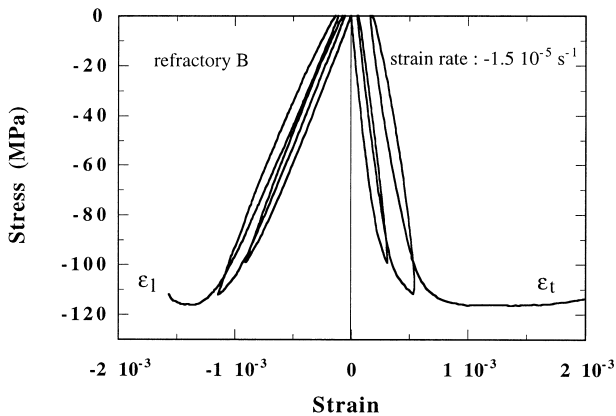

Fig. 3. Compression behaviour for material B under load-deloading pathes.

Table 2
Compression properties of magnesia-carbon refractories

Materials	MgO-C resin binder (A)	MgO-C pitch binder (B)
Young's modulus E_c (GPa)	10.6	102
Poisson's ratio ν	0.16	0.24
Compression strength σ_{cr} (MPa)	−27.2	−115.6
Maximal strain ϵ_{max}[a]	−4.9 10^{-3}	−1.62 10^{-3}

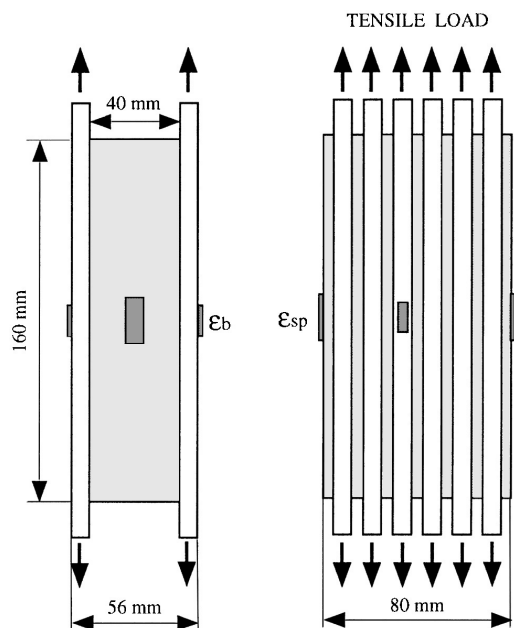[a] Strain measured at the minimum stress of the curve.

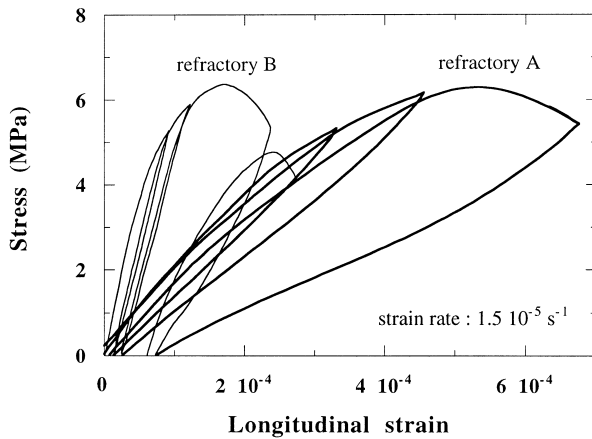Fig. 4. Specimen for the tensile test.

Fig. 5. Tensile behaviour for material A and B.

However, this technique can be used for comparison between different refractories.

The mechanical properties for the two kinds of material are reported in Table 3. The value of Young's modulus E_t corresponds to the secant modulus that was measured for an axial strain of $5\ 10^{-5}$.

As shown in the past,[13] the maximum stress deduced from this test is always higher than the one from the direct tensile test. This is the consequence of the coalescence of many microcracks and of their stable propagation in the specimen up to the peak. On the contrary a classical tensile test should be used on the occurrence of a single crack propagating suddenly as soon as it is created.

3.3. Discussion

3.3.1. Young's modulus

A significant discrepancy was observed between Young's modulus deduced both by compression and tensile tests E_c and E_t. In order to explain this difference, other tests were performed.

The ultrasonic test is currently used in the refractory industry to check the quality of materials. The standard apparatus allows for the measure of longitudinal wave speed value V_L and shear wave speed value V_S. Under the assumptions of homogeneity of the material and linear elasticity, the value of Young's modulus E_{us} and

Poisson's ratio v_{us} can be deduced by the classical formulae:[14]

$$E_{us} = \rho V_S^2 \frac{3V_L^2 - 4V_S^2}{V_L^2 - V_S^2} \quad \text{and} \quad \frac{1}{2}\frac{V_L^2 - 2V_S^2}{V_L^2 - V_S^2} \tag{1}$$

In the tests, at first, the acoustic velocities were measured in the three axis of the specimens. Material A exhibited a light anisotropy: the longitudinal wave speed was seven per cent higher in the axis corresponding to the mechanical loading during the manufacturing process than in the other axis. This anisotropy is probably due to microcracks which appeared according to preferential axis of the brick during the casting and the heat treatment or by a slight anisotropy of the distribution of graphite flakes occurring at the time of the pressure of bricks.

In material B no anisotropy was detected. The difference of the wave speed in the three axis was less than 1%. This can be explained by the fact that during the manufacturing and the heat treatment, the viscosity of the carbonous binder was very high, so that the molding matrix healed itself when microcracks opened.

The slight anisotropy in material A was not considered in this study. Care was taken to machine the specimen always with respect to the brick axis. The mean values of Young modulus E_{us} are reported in Table 4.

It appears that a direct connexion does not exist between Young's modulus E_{us} and the other Young's modulus. For the two materials E_{us} was higher than the highest Young's modulus (E_{us} and E_t) found by the uniaxial tests and that even for material B which seemed macroscopically linear elastic for small strains.

Many factors may explain these discrepancies.

- An effect of the heterogeneity of the material that induced wave dispersion. In our case, the imposed frequency of the transducer was close to 1 MHz, but due to the wave attenuation the received signal was centred around 300 Hz. It resulted in the wave length being larger than the greatest size of the grain (5 mm) which excluded this phenomenon.
- A viscoelastic behaviour of the material. But both mechanical cycling loading within the range $10^{-2}-10^2$ Hz corresponding to strain rate $5.10^{-7}-5.10^{-3}$ and relaxation tests did not allow for detecting viscosity for these refractories. Due to

Table 3
Tensile properties of magnesia-carbon refractories

Material	MgO-C resin binder (A)	MgO-C pitch binder (B)
Young's modulus E_t (GPa)	25.2	69.8
Tensile strength σ_{tr} (MPa)	6.5	6.3
Maximal strain ϵ_{max}[a]	$5.0\ 10^{-4}$	$1.64\ 10^{-4}$

[a] Strain measured at the maximum stress of the curve.

Table 4
Acoustic velocities and Young's modulus deduced by US measurements

Material	V_L (m/s)	V_S (m/s)	E_{us} (GPa)
MgO-C resin binder (A)	3400	2123	30.1
MgO-C pitch binder (B)	6483	3884	113

the pyrolysis of resin of pitch during the heat treatment the initial viscous carboneous phase was changed into a rigid carbon skeleton which was not very sensitive to strain rate effects. It is possible that the viscoelastic phenomenon occurs for frequencies higher than 10^2 Hz.

Thus, other physical causes must be found to explain the differences in stiffness revealed by compression and tensile tests. To this end, a prismatic specimen was glued on the grips of the testing machine to study both tensile-compression behaviour of the refractories for small deformations and to measure with great accuracy its stiffness. The specimen was equipped with strain gauges on its faces. The tension/compression test was performed at a low strain rate ($|\dot{\varepsilon}| \leqslant 10^{-6} s^{-1}$).

The previous load cycling, applied to material A during the test, is shown in Fig. 6. One can see that even for extremely small strains, typically lesser than $4 \ 10^{-5}$ absolute value, the stress versus strain curve exhibited an hysteretic loop.

In the following loads shown in Fig. 7, higher strain levels were applied to the specimen. At first, a monotonic
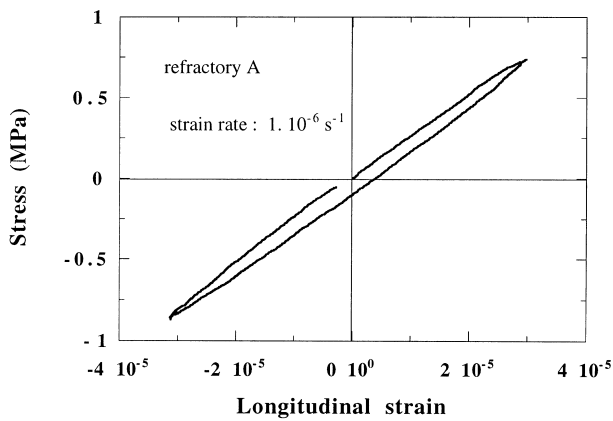

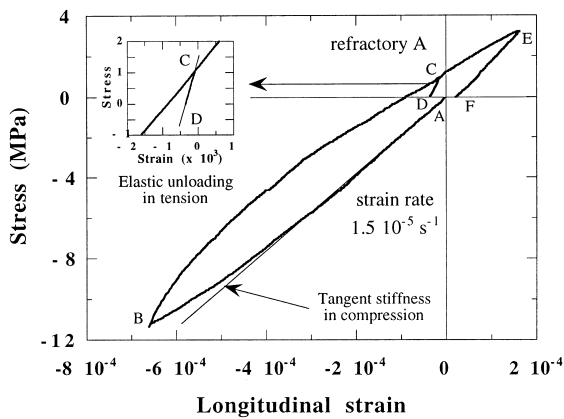Fig. 6. Non linear behaviour under very small strains for material A.

Fig. 7. Young's modulus definition in tension and compression for material A.

compression load was performed (path AB) and revealed that non-linearity increased with strain. Then the specimen was unloaded and loaded under tensile stress (path BC). The true elastic modulus was given only by the very small elastic unloading path CD. Finally, the specimen was once again loaded in tension (path DCE). The behaviour remained linear up to C then became non linear (path CE). One can see that the stiffness in both CD was nearly 2.5 times higher than the one observed in the compression load.

The determination of Young's modulus was classically made for tensile strains between 0 and $5 \ 10^{-5}$ (one tenth of the elastic domain). On the contrary, in compression the usual measurements were made for larger strains, typical between 0 and -5.10^{-4}. This classical interpretation gave tangent modulus that differed from the true elastic modulus which was reached only for very small strains. Indeed during the mechanical loading the initial microcracks occurring in the material at the time of the manufacturing may open, slide or not, depending on the friction that existed between the lips of the cracks. These effects disturbed the measurement of the elastic moduli. Microplasticity and residual stresses may also introduce errors for higher strains.

Lastly, a complementary physical cause gives an explanation of the difference in Young's modulus deduced by compression-tensile tests.

For material B, $E_c \geqslant E_t$ was due to the fact that the opened microcracks were nearly closed. During the compression loading the cracks perpendicular to the load direction closed immediately and so the stiffness of the material increased first. The curve stress versus strain remained linear over strains that were largely higher than those used to measure Young's Modulus.

For material A, $E_c \leqslant E_t$. The microcracks were more open and, therefore, the closure of microcracks located perpendicularly to the load was more progressive and consequently the increase in stiffness was slower. The opposite effects of the microplasticity in the binder already mentioned and the reducing of the transverse stiffness due to the easier opening of the other oriented microcracks were added to the previous phenomenon. Thus, the combination of all these phenomena led to the lower value of E_c.

These effects are very important to keep in mind when the compression test is used to determine the stiffness of refractory and when building mechanical models. The tensile test is preferable for these reasons in identifying Young's modulus.

3.3.2. Ultimate strengths

In Table 5, the absolute value of the compression strength to tensile strength ratio is reported. Material B presented a high ratio and consequently a strong disymmetry between tension and compression while material A presented an appreciably lower disymmetry. This

Table 5
Absolute compressive strength to tensile strength ratio

Material	MgO-C resin binder (A)	MgO-C pitch binder (B)
Ratio	4.2	16.3

difference can be justified by the fact that (i) the pitch binder was lesser damaged by the manufacturing of the bricks and (ii) more brittle than the resin binder and the interface between the aggregates and the binder was stronger for material B than for material A.

4. Tensile behaviour by the three-point bend tests

4.1. Experimental set-up for room temperature

4.1.1. Loading device

The three-point bend test is a widely used test to determine the tensile strength, the so-called 'modulus of rupture' M.O.R., because it is easier to perform than the tensile test. It is quite suitable at high temperature. Nevertheless the experimental results are very sensitive to the boundary conditions (loading and supports) and minimal precautions must be taken.

On the other side, today this test is more and more often used to determine Young's modulus by measurement of the deflexion. But, as for usual ceramic specimen the deflexion is low, the measure is generally not very accurate.

For these reasons, in the device especially designed[6] and shown in Fig. 8, a particular attention is paid to the boundary conditions. The load is applied to the specimen through a roller which has a free rotation motion. The beam rests on two removable supports so that beams of different sizes can be tested. One of the rollers is made of two parts allowing it to revolve about the axis parallel to the specimen (long) axis. Thus, even if the specimen presented a planeity, defect no parasit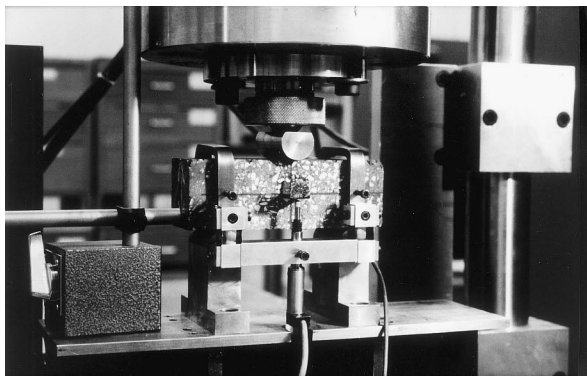e bend and twist occurred. This was checked by measuring the tensile strain on the bottom face of the specimen as shown in Fig. 9. One can see that the two gauges placed on the lower face of the specimen and on each side gave exactly the same information.

To measure the deflexion, usually a transducer is set on the frame of the testing machine and the displacement of the middle bottom part of the beam is measured. But as the expected deflexion of the beam was small (less than 50 μm), parasite effects like deformations near the supports and under the loading point and the deformation of the testing machine can not be neglected. The improvement consisted in measuring the real deflexion of the central line of the beam. Two reference points are fixed on the neutral axis of Sections 1 and 2. The grips allow the rotation of the sections of the beam without any disturbance on the measurement system. Two deformable parallelograms placed between the grips and the aluminium bar allow the x elongation of the beam. The transducer is fixed on this bar and its sensor is fixed on a thin plate glued on the neutral axis of the beam. This apparatus gives deflexion values with a high accuracy.

The bend tests were done on small prismatic specimens (50 × 50 × 200 mm) with a span between the supports equal to 150 mm.

4.1.2. Interpretation of the load-deflexion curve

In the classical theory of elastic beam, under plane stress assumption and the hypothesis of St Venant, for the three point bend test Young's modulus E is related to force F and deflexion f by the expression

$$E_f = \frac{Fl^3}{48If} \qquad (2)$$

where I is the moment of inertia of the cross-section and l the span. For a rectangular cross section (height h and breadth b), the moment of inertia is equal to $I = \frac{bh^3}{12}$.

Expression (2) is no longer correct when the span to height ratio is short and the plane stress condition no longer available. Indeed, the cross-section is submitted to distortion so that it is changed into a curved surface

Fig. 8. Experimental set-up for three point bend test at room temperature.
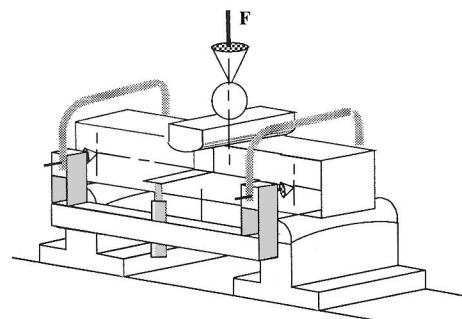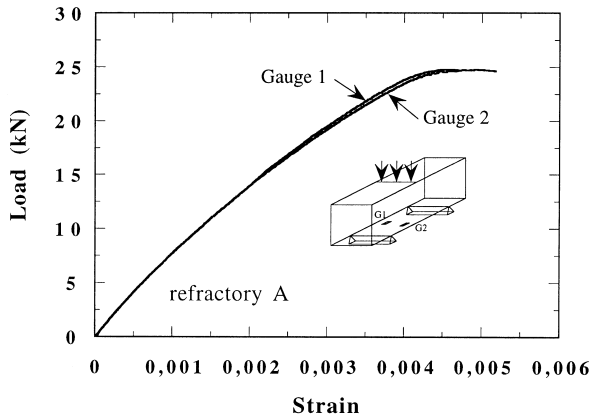
Fig. 9. Load versus strains measured with gauges.

instead of a plane surface as previous. Therefore it is necessary to introduce a correction parameter α to add the deflexions due to shearing and edge effects:

$$E_f = \frac{Fl^3}{48If}(1 + \alpha) \tag{3}$$

Different formulae of α were proposed in the literature (see Timoshenko)[15]. For prismatic beams, they read

$$\alpha = 3(1 + v)\left(\frac{h}{l}\right)^2 \tag{4}$$

$$\alpha = 2.85\left(\frac{h}{l}\right)^2 - 0.84\left(\frac{h}{l}\right)^3 \tag{5}$$

In formula (4) α accounts for the shear effect supposing that shear deformation is free. But because of the symmetry, close to the loading force warping will establish progressively. This leads to a later correction which is given by formula (5).

It is equal to 0.286 for the specimen and tends to zero for high values of $\frac{l}{h}$ (0.03 for a ratio of 10).

In the case of the specimen geometry tested, a comparison of these different formulae was made with the result of a finite element computation. It showed a good agreement of formula (5) with the numerical value.

4.1.3. Measurement of the tensile strength

The usual estimation of the tensile strength is made under the assumption of a linear elastic behaviour up to the failure of the specimen for $\sigma^{\max} = \sigma_t^{\max}$ and supposing the stress distribution under the load point is identical to that observed far from it. It leads to the following definition of the modulus of rupture *M.O.R.*

$$\sigma_t^{\max} = M.O.R. = \frac{F_r lh}{8I} \tag{6}$$

where the value of F_r corresponds to the ultimate load prior to the failure of the beam.

A finer analysis[16] shows that the distribution is not linear in the cross-section where the load is applied. The tensile strength $\sigma_t^{\max}$ is lower than the value estimated by expression (6) and is given by

$$\sigma_t^{\max} = \frac{M.O.R.}{\beta_1} \quad \beta_1 = \frac{1}{1 - 0.1773h/l} \tag{7}$$

The correction for the specimen geometry is β_1 equal to 1.06.

The effect of the ''visible'' non symmetric linearity of behaviour in tension and compression can also be estimated using the classical theory of beam. For example, Schach[17] calculates the $\sigma_t^{\max}$ using two different Young's moduli.

It is also possible to deduce the tensile strength considering a non linear behaviour. For example Planas and coworkers[18] propose the following expression for a quasi-brittle material.

$$\sigma_t^{\max} = \frac{M.O.R.}{\beta_2} \quad \beta_2 = \max\left(1 + \frac{2s}{h} - \frac{4k}{k + (h/s - 1)^2}\right) \tag{8}$$

where s is the depth of the damage zone, $k = E_s/E$ and E_s is the softening modulus. For $k = 0.5$ β_2 is equal to 1.3.

In this case, the maximal stress in the bottom face is not obtained for the maximal load as shown later.

4.2. Results

The mean value of Young's modulus and the *M.O.R.* of the refractories given by the expressions (5) and (6) are reported in Table 6.

4.2.1. Young's modulus

The correlation between the bending test and the tensile test was good for material B which had a brittle behaviour.

Young's modulus E_f of material A was located between the value of compression and tension tests ($E_c = 10.6$ GPa and $E_t = 25.4$ GPa). As in bend tests the zone in compression had the same size as the zone under tension before degradation occurred, it stood to reason that E_f was an average value. Young's Modulus deduced by the gauges stuck on the bottom face of the specimen was equal to 24 GPa which was close to E_t and showed that this measure was more accurate. Unfortunately, this measurement is not adapted for tests under high temperatures.

4.2.2. Modulus of rupture

The strength given by the three-point bend test was higher than the tensile strength: 90% for material A and 14% for material B. For the material (A), this ratio is near to that found by L'Hermite[19] in concrete.

Table 6
Tensile properties of magnesia-carbon materials by bend test

	MgO-C resin binder (A)	MgO-C pitch binder (B)
E_f (GPa)	18.6	69
M.O.R. (MPa)	7.4	13.5

The discrepancies can be explained by several reasons:

- The non homogeneous initial state of the material because the heat treatment may affect differently the specimens for bend tests than the specimens for tensile tests.
- Probabilistic effects (volume scale, defects, heterogeneity of the stresses) which affected the probability of failure as already shown by Hild.[20] The material is all the more sensitive to these effects as its behaviour is brittle (refractory B was more sensitive to these effects than refractory A)
- The non linear behaviour observed for these materials even for small strains.

4.3. Numerical simulations of the three-point bend test

The effects of the non-linearity of the behaviour on the estimation of the tensile strength by the three-point bend test have been analysed with a finite element program ABAQUS.[21] The simulations have been made within a thermomechanical model of behaviour (including damage and plasticity) which is briefly described below.

4.3.1. Constitutive equations

The mechanical model developed for the refractories tested is an extension of a model proposed by Comi et al.[22] Within the frame of thermodynamics of irreversible processes, a set of state variables permits to characterize the main microscopical phenomena observed (isotropic elasticity, progressive degradation and appearance of permanent strains).

Elastic strains $\underline{\varepsilon}^e$, permanent strains $\underline{\varepsilon}^{in}$ and a scalar damage variable d are introduced. The total strain tensor $\underline{\varepsilon}$ is given by $\underline{\varepsilon} = \underline{\varepsilon}^e + \underline{\varepsilon}^{in}$.

The law of elasticity coupled with damage reads

$$\underline{\sigma} = (1 - d)\left[K(\varepsilon_v^{in} - \varepsilon_v^{in})\underline{1} + 2G(\underline{e} - \underline{e}^{in}) \right] \quad (9)$$

where $\underline{e}$ represents the deviatoric part of the total strain tensor and subscript v refers to the volumetric part of the tensor. The scalars K and G correspond to the bulk and shear moduli.

The elasticity domain of these materials is represented by an ellipsoid in the stress space defined by

$$f = \frac{I_1^2}{18K(1 - d)^2} + \frac{J_2}{2G(1 - d)^2} + B(d)I_1 - R(d) = 0 \quad (10)$$

In this expression I_1 and J_2 represent the classical first and second invariants of the stress tensor and $B(d)$ and $R(d)$ are functions of damage and identified from tensile and compression tests. These functions reproduce the hardening-softening behaviour and the dissymmetry between tension and compression.

The evolution laws for damage and permanent strains are derived from the viscoplasticity theory. They read

$$\dot{d} = \Phi = \frac{I}{\mu}\left\langle \phi(f, \underline{\sigma}, d) \right\rangle^n \quad (11)$$

$$\underline{\dot{\varepsilon}}^{in} = \Phi \underline{C}(d, \underline{\sigma}) \quad (12)$$

where $\langle . \rangle$ represents the MacLaurey bracket. Function Φ reproduces the intensity of the viscous effect. It mainly depends on two classical "viscous" parameters, an exponent n and a coefficient μ. $\underline{C}$ is a tensorial function of $\underline{\varepsilon}$ which is in connection with the mechanisms of plasticity or damage. More details on the constitutive equations may be found in Ref. 6. This model was identified using the tensile and compression tests and relaxation tests.

As an example, one gives, in Fig. 10, the response of the model for uniaxial tension for the refractory A with resin binder. The strain rate used for the identification was equal to 10^{-5} s^{-1}. The unloading pathes were well reproduced except for the hysteresis for which a more sophisticated model would be needed (including friction as a micromechanism).

4.3.2. Numerical computations

This model was used to simulate the three-point bend test. The specimen tested was a prism (50 × 50 × 200 mm). Due to the symmetry of both the geometry and the loading only a quarter of the specimen was meshed.
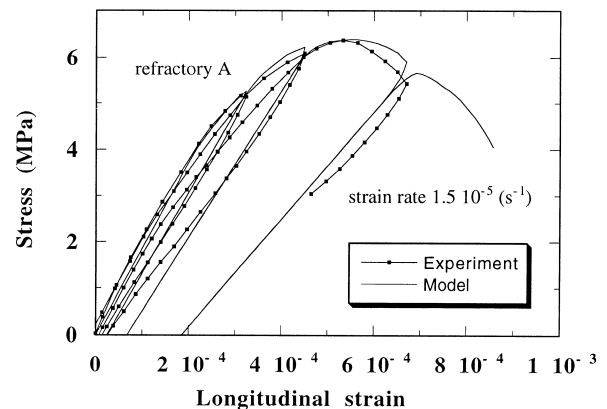

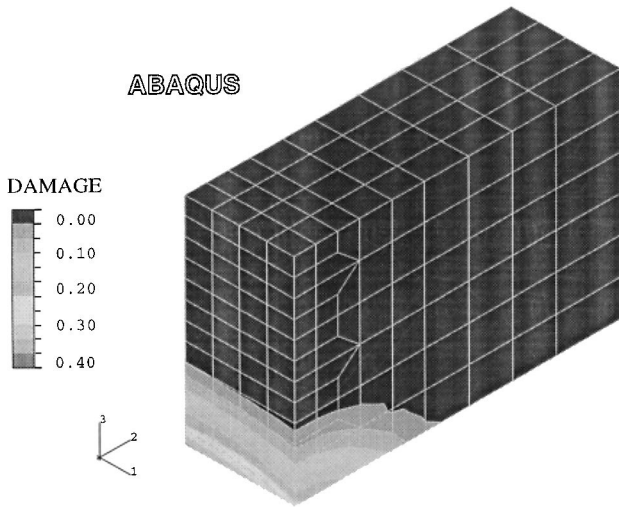Fig 10. Stress vs. strain curves under tensile load: model and experiment.

Fig. 11. Mesh of a quarter of the specimen and damage map at the end of the load.
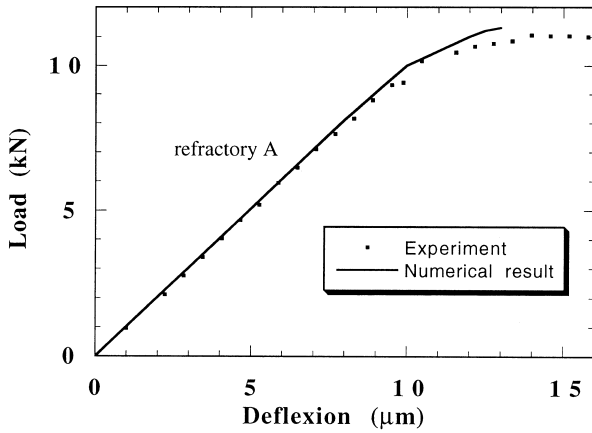

Fig. 12. Load versus strain for the three-point bend test.

Fig. 13. Load deflection curve deduced by numerical computations.

Fig. 11 shows the damage map for the maximum load, stage at which the computation had stopped for numerical reasons (loss of unicity of the solution). Damage is visible in a large area on the right of the section under the loading point.

The load deflection curve is given in Fig. 12 where the deflection corresponded to that measured during the test. One can notice an apparent linear part followed by a non linear regime due to the progression of damage from the lower part of the beam to the upper part.

The maximum load recorded in this numerical test is noted F_{num}. If this value is used to compute a tensile strength noted $\sigma_{t\text{-bending}}$ [using Eq.(6)] a value of 13 MPa is obtained. This value does not match with the tensile strength σ_t which is equal to 6.5 MPa. This corresponds to what has been observed in the experiments.

The evolution of the longitudinal tensile stress in the low part of the mesh under the load is also recorded (Fig. 13). The tensile stress increases up to a value of 6.5
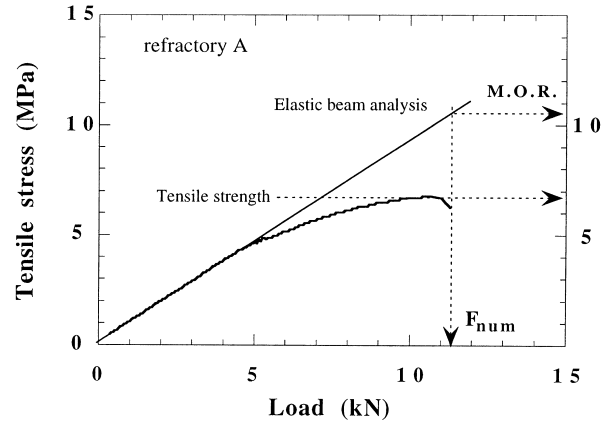
MPa that corresponds to the tensile strength identified from the uniaxial tensile test. It proves that the local state of stress is purely uniaxial at that point.

In Fig. 13 the straight line reported corresponds to a linear elastic beam finite element simulation up to the maximum load F_{num}. The maximum tensile stress reached in this case gives a tensile strength of 10 MPa which is lower than the 13 MPa obtained by Eq. (6). For short span to height ratio the classical *M.O.R.* overestimates the maximum tensile stress and it is necessary, at least, to estimate it with a finer elastic analysis as that proposed by Timoshenko[16] using Eq. (8). The non linear behaviour of the refractory is responsible of the difference between the F.E.M. estimation of *M.O.R.* and the true tensile strength of the material. For such materials, it seems better to estimate the tensile strength using the approach proposed by Planas et al.[18] considering Eq. (6). When the material is brittler this difference decreases, but due to the heterogeneity the probabilistic effects are more important.

It is very difficult to give a rule to determine the ultimate tensile strength from this test because the effect of the damaged tensile region on the global load displacement curve is not constant. It depends on the ratio between tensile and compressive strength and on the brittleness of the refractory.

5. Conclusion

Magnesia-carbon based refractory materials exhibit a non linear behaviour even for extremely low strains that perturb the determination of the elastic properties such as Young's modulus. At first it has been shown that the elastic domain is limited to strains below 10^{-5}. The ultrasonic measurements of elastic constant gives higher values due to heterogeneity of the material and to viscous effect even if they cannot be detected by classical tests within the range 10^{-2}–10^2 Hz.

The special tensile test enabled to obtain the hardening softening behaviour in tension. Then an experimental set-up has been developed to perform a three-point bend test with a correct measurement of the beam deflexion. Young's modulus derived from this experiment is well in accordance with those given by tension. The *M.O.R.* does not give a correct estimation of the tensile strength as measured in tension in case of a large hardening in compression. It is not possible to detect this phenomenon without local strain measurements (in the low part of the specimen) or comparison between experiments and numerical computations based on non linear constitutive equations.

Acknowledgements

References

1. Bisson, G. and Thémines, D., Etude par éléments finis du comportement de pièces réfractaires sollicités thermiquement. Colloque Réfractaires et sollicitations thermomécaniques, S.F.C., 14–15 Mai 1990, Paris, France (in French).

2. Hasselman, D. P. H., Unified theory of thermal shock fracture initiation and crack propagation in brittle materials. *J.A.C.S.*, 1965, **52**(11), 601–604.

3. Rand, B. and Mc Enaney, B., Carbon binders from polymeric resins and pitch. Part I: pyrolysis behaviour and structure of the carbons. *Br. Ceram. Trans. J.*, 1985, **84**, 157–165.

4. Lubala, N. C., Rand, B. and Brett, N. H., Effect of carbon binders on the development of porosity in MgO-Graphite composite refractories. *Br. Ceram. Trans. J.*, 1988, **87**, 164–167.

5. Fitchett, A. M. and Wilshire, B., Mechanical properties of carbon-bearing magnesia, Parts I, II and III. *Br. Ceram. Trans. J.*, 1984, **83**, 54–76.

6. Robin, J. M., Comportement thermomécanique des céramiques réfractaires, Thèse de doctorat, Université Paris 6, 1995 (in French).

7. Mazars J., Application de la mécanique de l'endommagement au comportement non linéaire et à la rupture du béton de structure, Thèse de doctorat d'Etat, Université Paris 6, 1984 (in French).

8. Evans A. G. Perspectives on the development of high-toughness ceramics. *J. Am. Ceram. Soc.*, **73**, (2), 187–206, 1990.

9. Cooper C. F., Alexander I. C., and Hampson C. J., The role of graphite in the thermal shock resistance of refractories. *Br. Ceram. Trans. J.*, 1985; **84**, 57–62.

10. Bazant Z. P. and Pijaudier-cabot G., Measurement of characteristic length of non local continuum, *J. Engng Mechanics, ASCE*, 1985; **115**, 4, 755–767.

11. Mazars J. and Berthaud Y., Une technique expérimentale appliquée au béton et pour créer un endommagement diffus et mettre en évidence son caractère unilatéral, *Comptes Rendus Acad. Sci.*, 1989; t. **308**, (série II), 579–584 (in French).

12. Boudon-Cussac, D., Hild, F. and Pijaudier-Cabot, G., Tensile damage in concrete: analysis of experimental technique. *J. Eng. Mech*, 1999, 906–913.

13. Breysse, D. and Schmitt, N., A test for delaying localisation in tension, numerical investigation. *Cement and Concr. Res.*, 1991, **21**, 15.

14. Krautkramer, J. and Krautkramer, H., *Ultrasonic testing of materials*, 2nd ed. Springer-Verlag, Berlin Heidelberg New York, 1977.

15. Timoshenko, S., *Strength of materials*. D. Van Nostrand Company, Princeton, New Jersey, 1955.

16. Timoshenko, S. and Goodier, J. N., *Theory of elasticity*, 2nd ed. Mc Graw-Hill, New York, 1951.

17. Schacht Ch, A., *Refractory linings: thermomechanical design and applications II. Mechanical engineering*. Dekker M, New York, 1995.

18. Planas, J., Guinea, G. V. and Elices, M., Rupture modulus and fracture properties of concrete. *Fracture Mechanics of Concrete Structures, Vol. 1,* ed. F. H. Wittmann. Aedificatio Publishers, Freiburg Germany, 1995, pp. 95–110.

19. L'Hermite, S., Influence de la dimension absolue sur la résistance en flexion. *Ann. I.T.B.T.P.*, 1973; **309**, 39–41 (in French).

20. Hild, F., De la rupture des matériaux à comportement fragile. Thèse de Doctorat, Université Paris 6, 1992 (in French).

21. Hibbitt, Karlson and Sorensen, Code de Calcul Abaqus, version 5.3, 1993.

22. Comi, C., Berthaud, Y. and Billardon, R., Identification of elastic plastic behaviour from localisation measurements. *Eur. Journal of Mechanic/Solids*, 1995, **1**, 19–43.